Heterogeneous Polyamide 66/Syndiotactic Polystyrene Blends: Phase Structure and Thermal and Mechanical Properties

J. Kolařík,[1] L. Fambri,[2] M. Šlouf,[1] D. Konečný[3]

[1]*Institute of Macromolecular Chemistry, Academy of Sciences of the Czech Republic, 162 06 Prague 6, Czech Republic*
[2]*Department of Materials Engineering and Industrial Technologies, University of Trento, 38050 Trento, Italy*
[3]*Research Institute of Inorganic Chemistry, 400 60 Ustí nad Labem, Czech Republic*

Received 9 February 2004; accepted 22 July 2004
DOI 10.1002/app.21496
Published online in Wiley InterScience (www.interscience.wiley.com).

ABSTRACT: The structural and physical properties of polyamide 66 (PA66)/syndiotactic polystyrene (sPS) blends were studied with electron microscopy, wide-angle X-ray scattering (WAXS), differential scanning calorimetry (DSC), dynamic mechanical thermal analysis, and tensile creep, stress–strain, and impact measurements. Attention was primarily concentrated on blends with sPS weight fractions (w_2) in the range of $0 < w_2 \leq 0.50$. DSC and WAXS showed that the integral crystallinity of the PA66 and sPS components in the blends was virtually unaffected by the blend composition. Polymorphism of sPS was observed for blends with $w_2 \geq 0.50$. Blends with $0.40 \leq w_2 \leq 0.60$ consisted of partially cocontinuous components; otherwise, particles of the minority component were dispersed in the continuous majority component. The compatibilizer enhanced interfacial adhesion so that no debonding of the components in the fractured blends was observed. The compliance and creep rate of the blends at room temperature decreased proportionally to the sPS fraction; a corresponding increase in the storage modulus (E') was observed in the 25–100°C interval. However, E' (125°C) noticeably declined with w_2 and thus showed that sPS did not improve the dimensional stability of the blends at elevated temperatures. The yield strength consistently grew with w_2, whereas the yield strain dropped markedly; blends with $w_2 \geq 0.60$ were brittle, showing very low values of the ultimate properties. The stress at break, strain at break, and tensile energy to break displayed some local maxima at $0.25 \leq w_2 \leq 0.30$, whereas the tensile impact strength steeply decreased. J Appl Polym Sci 96: 673–684, 2005

Key words: blends; mechanical properties; polyamides; polystyrene; syndiotactic; structure-property relations

INTRODUCTION

New polymer materials with remarkable properties, such as high glass-transition temperatures (T_g's), high melting temperatures (T_m's), heat resistance, chemical resistance to common solvents, low moisture uptake, high water barriers, good mechanical properties, and transparency, are traditional objects of basic and applied material science. Syndiotactic polystyrene (sPS) is a semicrystalline polymer that attracts much attention[1–8] because of its high T_m (≅285°C), rapid crystallization, and high crystallinity and modulus; on the other hand, its T_g (≅100°C) is approximately equal to that of atactic polystyrene (PS). Mainly, the heat resistance and chemical stability allow potential applications of sPS at elevated temperatures. The crystalline phase of sPS has been the subject of many studies,[1–8] which have shown the coexistence of several crystalline modifications (polymorphism), although under ordinary conditions, the α modification (a planar all-trans form with a planar zigzag backbone structure) dominates.[3] The stiffness of crystalline sPS has been ascribed to intrachain interactions involving bond bending and stretching. Practical applications of sPS are limited by its inherent brittleness at ambient temperatures because sPS does not show any crazing or shear yielding (i.e., plastic microdeformations) before fracture.[3] Mainly for this reason, sPS is blended with other thermoplastics to eliminate this deficiency. However, as the processing temperature of sPS is necessarily higher than its T_m, polymers used for blending have to sustain a processing temperature of approximately 290°C, and this may limit the choices.

So far, sPS has been reported to be miscible with poly(phenylene oxide)[9–11] and tetramethyl bisphenol

Correspondence to: J. Kolařík (kolarik@imc.cas.cz).
Contract grant sponsor: Grant Agency of the Academy of Sciences of the Czech Republic; contract grant number: A4050105 (to J.K.).
Contract grant sponsor: Grant Agency of the Czech Republic; contract grant number: 106/02/P029 (to M.Š. for electron microscopy studies).
Contract grant sponsor: Ministry of Education, Youth, and Sports of the Czech Republic; contract grant sponsor: LN 00B142 (for the synthesis of the compatibilizer at the Research Institute of Inorganic Chemistry).

A polycarbonate.[12] However, to suppress the brittleness of sPS, small particles of immiscible elastomers may be incorporated (10–20%) that initiate plastic microdeformations. To this end, sPS has been blended with ethylene–propylene rubber,[13] thermoplastic polyurethane,[14] a hydrogenated styrene–butadiene–styrene block copolymer (Kraton G1651),[15] and a styrene–ethylene/butene–styrene block copolymer (Kraton G1652).[16] Moreover, blends of sPS with various thermoplastics have recently been prepared via melt mixing, such as sPS/high-density polyethylene (HDPE)[17,18] and sPS/polyamide 6 (PA6).[19,20] The latter has been mainly focused on the efficiency of styrene/glycidyl methacrylate copolymers as compatibilizers. On the other hand, blends of sPS with polypropylene (PP) have been prepared through the polymerization of styrene and propylene with a Ziegler–Natta catalyst along with a novel electron donor.[21]

As expected, a crucial problem of sPS blends is the preparation of efficient compatibilizers leading to a fine phase structure and sufficient interfacial adhesion between dissimilar components. Poly[styrene-*block*-(ethylene-*co*-butene)-*block*-styrene] (SEBS) triblock copolymers, used in HDPE/sPS blends, are suitable, but they account for a significant reduction in the crystallinity of both components.[18] Nonetheless, the heat resistance of HDPE/sPS blends has been considerably improved by the incorporation of 20 wt % sPS. Although no interfacial adhesion has been found in blends without any compatibilizer, the addition of SEBS markedly promotes adhesion and leads to finer phase structures.[17] sPS/PA6 blends have been efficiently compatibilized by sulfonated sPS[19] or by styrene/glycidyl methacrylate copolymers.[20] The compatibilizers reduce the sPS domain size and improve the interfacial adhesion. sPS has also been tested as the matrix of nanocomposites with an organophilic clay of montmorillonite.[22,23]

Our primary intention was to prepare polyamide blends with a cocontinuous reinforcing sPS component, which could impart better dimensional stability to the blends at elevated temperatures. Numerous studies[24–32] have shown that a partially cocontinuous component affects the physical (mechanical) properties of blends much more than a dispersed component; that is, it accounts for a higher modulus, yield strength (S_y), resistance to creep, and so forth. It is also known[33,34] that a component with a lower relative viscosity in the melt shows a higher propensity for forming a cocontinuous phase. For this reason, we decided to use a polyamide with a viscosity higher than that of sPS to lower the critical volume fraction (the percolation threshold) of sPS in the blends, that is, to prepare blends with partially continuous sPS at volume fractions of less than 0.5. Our extensive preliminary tests indicated that available types of hydrolytic PA6 had a low melt viscosity, whereas alkaline PA6[35] had an appropriate viscosity, but its thermal stability was not sufficient at the processing temperature of about 285°C in a Brabender mixer and the following compression molding (microbubbles formed, probably as a result of this equilibrium amount of the monomer). To avoid the latter problem, we switched over to polyamide 66 (PA66), selecting an available product with a high molar mass. The objectives of this study were (1) to prepare compatibilized PA66/sPS blends showing good interfacial adhesion of the cocontinuous components, (2) to analyze their phase structure and crystallinity, and (3) to estimate the effects of the phase structure on the resulting mechanical properties.

EXPERIMENTAL

Materials

The polyamide Zytel E51HSB NC010 (DuPont, United States) is a heat-stabilized, high-molar-mass PA66 resin suitable for molding and extrusion applications. Its density is 1.14 g/cm^3, its T_m is 263°C, and the temperatures recommended for its processing are 280–305°C.

sPS, produced under the trade name Questra QA 101, is a product of Dow Plastics (Dow Europe S.A.). It has a density of 1.05 g/cm^3, a T_g of approximately 100°C, a T_m of 270°C (Dow test), and a melt-flow rate (at 300°C and 1.2 kg; ISO 1133) of 8 g/10 min.

So far, PA/PS blends have been successfully compatibilized with functionalized polymers miscible with PS[36–38] or with copolymers of styrene with monomers containing suitable reactive groups, such as carboxyl[39] and epoxy[40] groups. In this work, we used poly(2,6-dimethyl-1,4-phenylene oxide) (PPO) functionalized with fumaric acid in the process of reactive melt extrusion. The preparation of the compatibilizer was based on methods described earlier.[36–38] We used the following materials: (1) PPO (Asapryl 48, ASAP, Neratovice, Czech Republic; fine powder, weight-average molecular weight $\approx$ 41,000 g mol^{-1}), (2) 2,3-dimethyl-2,3-diphenylbutane (Perkadox 30, Akzo Chemicals B.V., Amersfoot, The Netherlands), and (3) fumaric acid (Pfizer & Co., New York, NY; fine granulate, purified). The functionalization of PPO was carried out with a laboratory single-screw extruder (type 015 extrusiometer, Berstorff; length = 40 cm, length/diameter = 20, three separately thermostated zones). The screw speed was set at 70 rpm, and premixed reaction components (500 g of PPO, 17.8 g of fumaric acid, and 5.0 g of 2,3-dimethyl-2,3-diphenylbutane) were fed into the extruder at a rate of approximately 10 g/min. The entrance zone was kept at 320°C; the other two zones were kept at 310°C. The fiberlike extrudate was cooled in ambient air and cut to obtain short fibers suitable for refeeding the extruder. Thus, the material was passed twice more through the extruder

TABLE I
DSC Data of the PA66/sPS Blends as a Function of the Composition

	First heating						Second heating			
PA66/sPS/C[a]	T_{g1}[b]	T_{g2}[b]	ΔH_c (J/g)[c]	T_m (°C)[d]	ΔH_m (J/g)	Cooling T_c (°C)[e]	T_{g1}	T_{g2}[b]	T_m (°C)[d]	ΔH_m (J/g)
100/0/0	42	—	3.3	264	67.3	231	63	—	264	79.1
90/10/1	43	nd	1.8	263	59.7	233	60	nd	263	73.8
85/15/1.5	44	nd	2.1	263	58.5	233	62	nd	263	70.5
80/20/2	35	94	2.3	263	56.0	232	59	101	263	67.9
75/25/2.5	42	99	2.3	263	54.9	233	60	102	263	64.5
70/30/3	36	102	1.6	264	51.6	232	62	107	263	61.4
60/40/3	44	100	1.4	263	47.0	231	65	103	264	56.7
50/50/3	42	101	1.0	263 (271)	44.7	(236) 231 (218)	64	101	263 (270)	51.0
40/60/3	41	101	0.8	263 (272)	41.4	235 (228, 217)	63	102	262 (271)	47.8
20/80/2	nd	98	0.1	(263) 271	33.9	235 (218)	nd	101	263 (272)	38.3
0/100/0	—	94	—	(265) 272	30.1	236	—	95	(263) 271	29.4

nd = not detectable; T_{g2} = glass-transition temperature of syndiotactic polystyrene.
[a] Blend composition (wt %); C = compatibilizer.
[b] Detected by DSC.
[c] During the first heating scan.
[d] Secondary peaks are in parentheses.
[e] Crystallization temperature in the cooling scan (secondary peaks are in parentheses).

under similar conditions. For the second passage, the temperature of the entrance zone was 318°C, and the temperature of the other zones was 312°C; for the third passage, the temperatures were 315 and 310°C, respectively.

Blend preparation

The compositions of the prepared series of PA66/sPS/compatibilizer blends are listed in Table I (in the text, only the PA66/sPS relative weight ratio is given to specify a blend). The amount of added compatibilizer was selected after a series of preliminary tests and a microscopic analysis of the obtained morphology. The polymers were mixed in the W50EHT mixer of a Brabender plasticorder (chamber volume = 50 mL, rate = 80 rpm, initial temperature = 285°C, mixing time = 6 min). The initial ratio of the PA66 and sPS torques at the processing temperature was about 2.3, which indicated a lower relative viscosity of sPS required for promoting sPS phase continuity. Three types of test pieces were produced. First, compression molding (Fontinje press; initial temperature = 285°C, initial pressure ≈ 3 MPa, pressing time = 4 min, time of cooling to room temperature ≈ 20 min) was used to obtain plates (100 mm × 100 mm × 2 mm) from which two types of test pieces were prepared: (1) strips (10 mm wide) for the measurements of the mechanical properties [dynamic mechanical thermal analysis (DMTA); creep] were sawn and (2) dumbbell specimens (65 mm long and 10 mm wide, reduced to 3 mm in the middle) were machined for the measurements of the tensile impact strength (TIS). Second, small dumbbell specimens (40 mm in gauge length, 1.5 mm thick, and 5 mm wide) were prepared by injection molding (microinjection-molding machine, DSM; barrel temperature = 280°C, injection pressure = 1.5 MPa) for stress–strain measurements.

Electron microscopy

Scanning electron microscopy (SEM) images and scanning transmission electron microscopy (STEM) images were obtained with a JEOL JSM 6400 scanning electron microscope and a Tescan TS 5130 Vega scanning electron microscope (equipped with a transmission adapter), respectively. SEM microphotographs showed the fracture surfaces of blends fractured in liquid nitrogen. Before being examined in the electron microscope, the samples were sputtered with platinum with a vacuum sputter coater (SCD, Balzers). All SEM microphotographs were secondary electron images taken at an acceleration voltage of 30 kV. STEM images showed RuO_4-stained ultrathin sections, which were prepared as follows: small pyramids were cut off and fixed in an ultramicrotome with a cryo attachment (Ultracut UCT, Leica); ultrathin sections were cut at −130°C, washed, transferred to Cu grids, and stained with RuO_4 vapor. The staining was based on the reaction of $RuCl_3 \cdot xH_2O$ with NaOCl, as described in the literature;[41,42] the staining times were approximately 60 min. Under these conditions, STEM microphotographs displayed bright PA66 components and dark sPS components. All STEM microphotographs were taken at an acceleration voltage of 30 kV.

Wide-angle X-ray scattering (WAXS)

The WAXS patterns were obtained with an HZG/4A powder diffractometer (Freiberger Praezisionsmechanik,

Freiberg, Germany). The total integral intensity (I_{tot}) and the integral intensity diffracted by the crystalline part (I_{cr}) of the samples were used[43] to determine the crystallinity (I_{cr}/I_{tot}). The size of the crystallites was estimated with the Scherrer equation:[43] $L_{hkl} = \lambda/\beta \cos \theta$, where L_{hkl} is the mean dimension of crystallites perpendicular to the planes (hkl), λ is the wavelength of the X-rays, β is the width of the reflection at the half-maximum intensity, and 2θ is the diffraction angle.

Differential scanning calorimetry (DSC)

A Mettler DSC 30 was used to perform two scans from 0 to 300°C. The heating rate and the cooling rate (between the scans) were 10°C/min. Tests were run under a nitrogen atmosphere (flow rate = 100 mL/min). Test specimens (ca. 20 mg) were used to ascertain T_g (the inflexion point corresponding to T_g of a crystalline polymer, whose fraction in the blends did not exceed 20%, was rather unclear), T_m, and the total melting enthalpy (ΔH_m). The crystallinity of the blend constituents was calculated with $\Delta H_{m1} = 190$ J/g and $\Delta H_{m2} = 53.2$ J/g for the crystalline phases of PA66[44] and sPS,[45] respectively.

DMTA

Measurements were performed with a DMTA Mk II instrument (Polymer Laboratories, Loughborough, United Kingdom) operated in the single-cantilever bending mode with 12 mm × 10 mm × 2 mm test specimens. The storage modulus (E') and loss modulus (E'') were measured from −100 to 150°C at a heating rate of 2°C/min with a dynamic displacement of 0.064 mm and a frequency of 1 Hz.

Tensile creep measurements

The tensile creep was measured with an apparatus equipped with a mechanical stress amplifier (lever; 10:1). Tests in the interval of 0.1–10,000 min (sometimes up to 15,000 min) were performed at room temperature, that is, 22–24°C. Mechanical preconditioning consisted of applying an elevated stress (for 100 min), which produced a strain higher than that expected in the intended experiment; the following recovery (before the registered creep was initiated) took place for about 22 h. The specimen dimensions were as follows: the initial distance between grips was 100 mm, and the cross section was 10 mm × 2 mm. The length of the creeping specimens was measured to an accuracy of 2 μm, that is, about 0.002%. The specimens used for the creep studies were stored for more than 6 months at room temperature to avoid any interfering effect of physical aging during the measurements.

Stress–strain measurements

An Instron 6025 tester was used to measure the tensile properties of the studied blends at room temperature. Dog-bone-shaped specimens with a gauge length of 50 mm (cross section = 5 mm × 1.5 mm) were tested up to fracture at a crosshead speed of 5 mm/min, that is, at a strain rate of 10%/min. Five specimens were tested for each blend.

TIS

TIS was measured at 23°C with a Zwick tester equipped with a special fixture for test specimens according to ISO 8256. Six specimens were tested for each material.

RESULTS AND DISCUSSION

Phase structure of the blends

The phase structure of the 90/10, 85/15, 80/20, 75/25, 70/30, 60/40, 50/50, 40/60, and 20/80 PA66/sPS blends was observed with SEM, STEM, or both. From a practical point of view, the most interesting blends were those with sPS as a minority component. SEM microphotographs of the fracture surfaces (Fig. 1) could be employed for a rough evaluation of the morphology and for a qualitative estimation of the interfacial adhesion. In all the PA66/sPS blends, the fracture at the temperature of liquid nitrogen was brittle, as documented by sharp fracture lines, which are dominating morphological features in Figure 1(a–d). The fracture advanced through both components, that is, not along the interface, and this suggested that the interfacial adhesion was strong enough to prevent the debonding of the components. Because of high interfacial adhesion, the resolution of the blend components was rather difficult: in all microphotographs [Figs. 1(a–d)], PA66 appears smoother and darker, whereas sPS looks coarser and lighter. It is possible to conclude that the 90/10, 85/15, and 80/20 blends [Fig. 1(a)] and the 75/25 and 70/30 blends [Fig. 1(b)] were composed of spherical particles of sPS in the continuous matrix of PA66. In the 60/40 blend [Fig. 1(c)], sPS formed rather big particles, showing some tendency to partial cocontinuity. The 50/50 blend [Fig. 1(d)] exhibited a clear cocontinuous phase structure. In the 40/60 blend, PA66 formed relatively big particles with some tendency to partial continuity, whereas the 20/80 blend consisted of smaller PA66 particles embedded in the sPS matrix. STEM microphotographs of the RuO_4-stained ultrathin sections (Fig. 2) provided a clearer view of the phase structure and confirmed the results of the SEM analysis; that is, the blends with a weight fraction of sPS (w_2) less than or equal to 0.3 [Fig. 2(a,b)] exhibited particulate morphology, whereas the blends with a w_2 range of $0.4 \leq w_2 \leq 0.6$

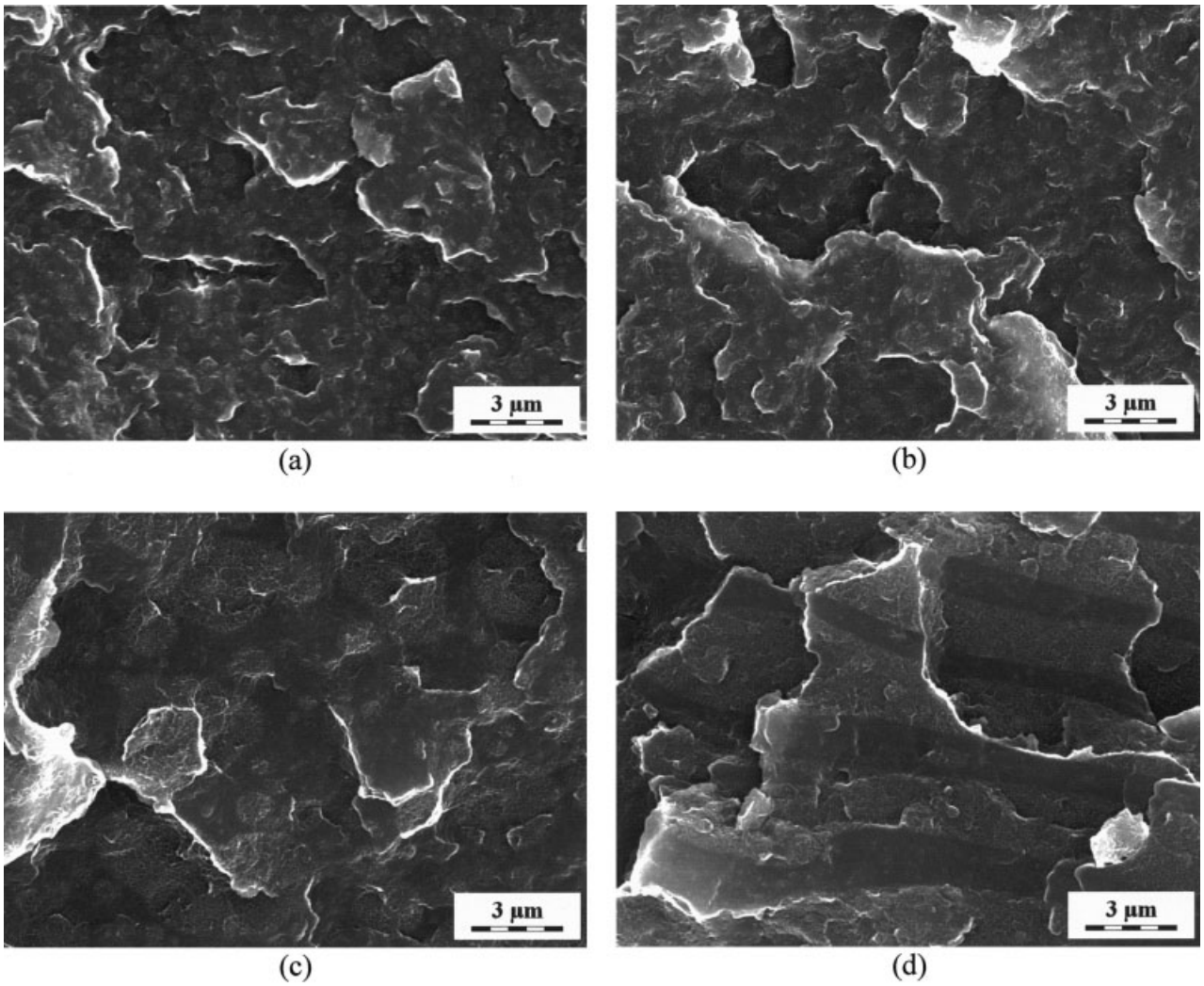

Figure 1 SEM microphotographs of fracture surfaces of PA66/sPS blends: (a) 80/20, (b) 70/30, (c) 60/40, and (d) 50/50 PA66/sPS.

[Fig. 2(c,d)] showed a partially cocontinuous morphology. Figure 2(c,d) displays an interesting detail not visible in the SEM microphotographs: PA66 contained small particles of sPS and vice versa.

Crystallinity of the blends: DSC and WAXS measurements

The properties of a blend constituent may differ from those of the starting polymer because of partial miscibility with other blend components, interactions with the compatibilizer, and induced changes in the structure (e.g., crystallinity). DSC shows (Table I) that PA66 and sPS had melting peaks at T_m = 264°C and T_m = 272°C, respectively. The crystallinity of the as-molded neat polymers was calculated after the subtraction of the enthalpy of secondary crystallization (ΔH_c) from the observed value of ΔH_m (Table I, first heating scan). In light of the indicated values[44,45] of ΔH_m of the crystalline phases, crystallinities of about 34 and 56% were obtained for PA66 and sPS, respectively. As PA66 and sPS melted at almost identical temperatures, it was evident that their melting peaks in the blends superposed (Fig. 3), and only ΔH_m (proportional to the total crystallinity) of a blend could be evaluated. Figure 4 shows that the values of $\Delta H_m - \Delta H_c$ for the as-molded blends did not obey the additivity (the rule of mixing) but were somewhat lower (cf. refs. 18, 20, and 46–48). The experimental data could be fitted with an empirical equation:

$$\Delta H_m - \Delta H_c = \Delta H_{m1} C_1 w_1 (1 - P_1 w_2) + \Delta H_{m2} C_2 w_2 (1 - P_2 w_1) \quad (1)$$

where w_1 and w_2 are the weight fractions (the percentage of added compatibilizer was neglected) and C_1 and C_2 are the crystalline fractions of PA66 and sPS, respectively, and P_1 and P_2 are empirical interaction parameters expressing a negative effect of component

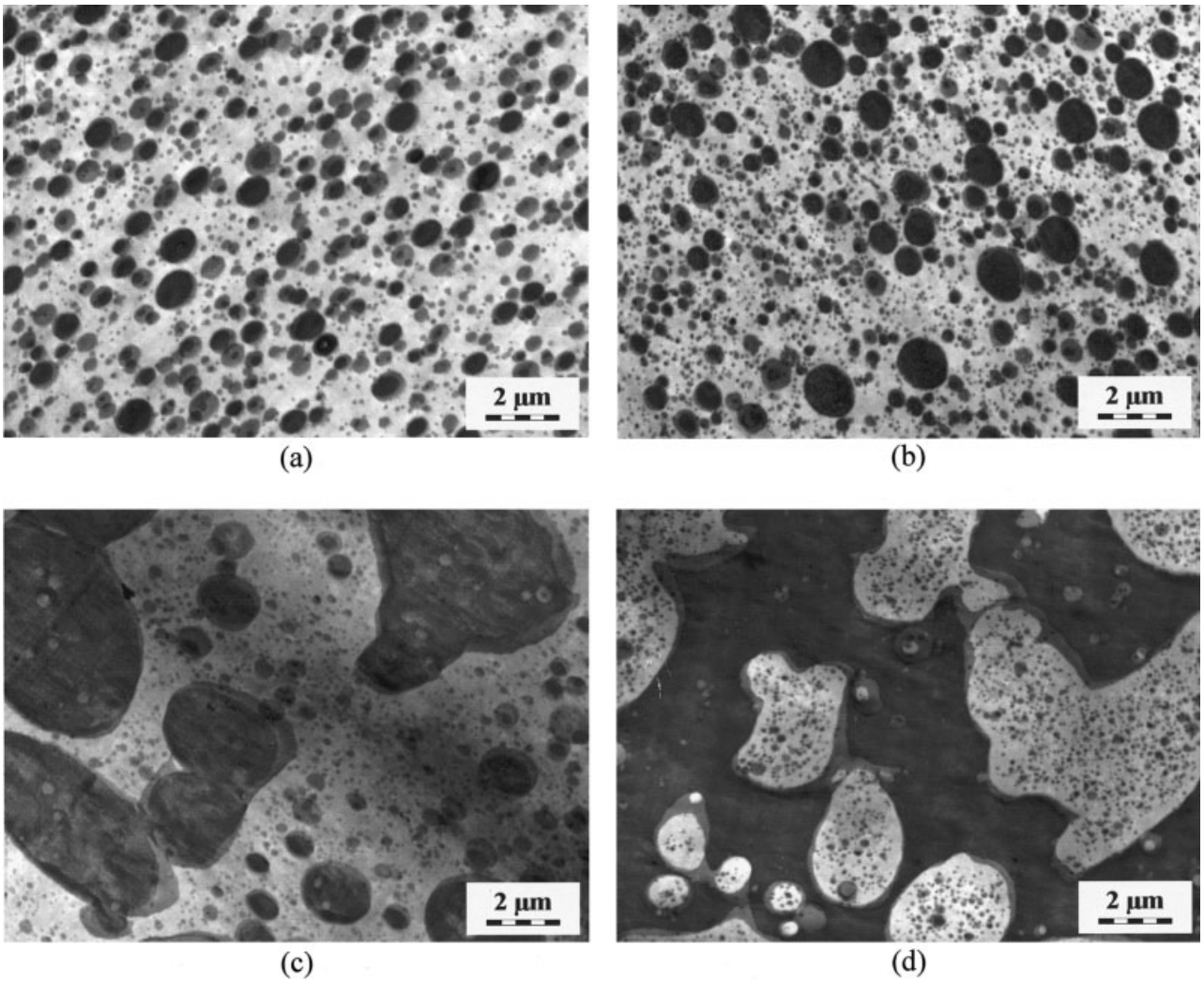

Figure 2 STEM microphotographs of RuO_4-stained ultrathin sections of PA66/sPS blends: (a) 80/20, (b) 70/30, (c) 60/40, and (d) 50/50 PA66/sPS.

2 on the crystallinity of component 1 and vice versa (the rule of mixing, visualized as a straight line, requires $P_1 = P_2 = 0$, which reflects zero interaction of the components; otherwise, $0 \leq P_1, P_2 \leq 1$.) $P_1 = 0.17$ and $P_2 = 0.33$ were obtained for the first heating scan performed with as-molded specimens characterized by $C_1 = 0.34$ and $C_2 = 0.56$. ΔH_m registered in the second heating scan, where $\Delta H_c = 0$ showed a dependence on the blend composition closer to linearity, that is, $P_1 = 0.10$ and $P_2 = 0.18$, but the values were noticeably higher than those in the first scan because C_1 was 0.42 and C_2 was 0.55. Higher values of the crystallinity and the absence of secondary crystallization in the second heating scan could be ascribed to more favorable conditions of crystallization (between the first and second heating scans) in comparison with those of the as-molded specimens. These results indicated that the crystallinity of PA66 and sPS was only slightly affected by the second component in the blends and but instead depended on the conditions of crystallization.

The cooling scan of the DSC measurements provided evidence of a complex crystallization process in the blends containing 50% or more sPS (Fig. 3 and Table I). Although blends with $w_2 \leq 0.4$ showed only one crystallization peak, blends with $0.5 \leq w_2 \leq 0.6$ displayed three peaks, and the 20/80 blend showed two peaks. The central peak at about 231°C, occurring in all the blends (except for 20/80), was proportional to the PA66 fraction and obviously corresponded to the crystallization of PA66. On the other hand, the peaks situated at a higher temperature (235–240°C) or at a lower temperature (ca. 217°C) could be attributed to sPS. It is well known that sPS can show three melting (or crystallization) peaks because of its polymorphism.[2,48–50] The multiple melting peaks of the studied blends may also be associated with a rather complex morphology of these blends with 50 or 60% sPS, in which cocontinuous components contained dispersed particles of the second component (Figs. 1 and 2).

The determination of the crystallinity with the WAXS method was rather complicated because of the

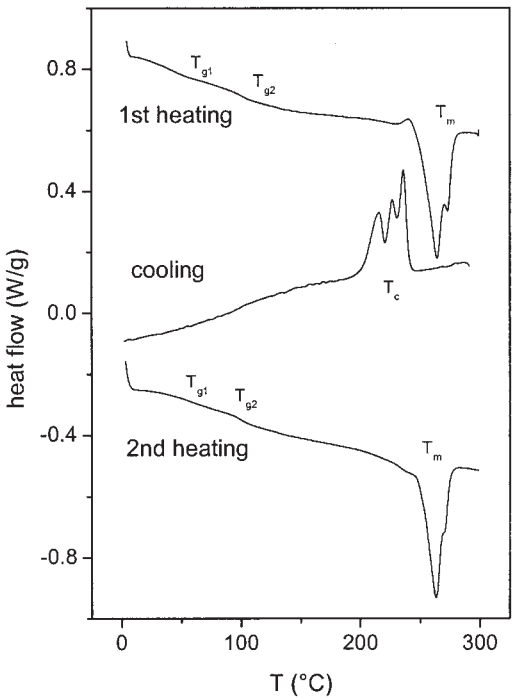

Figure 3 DSC thermograms of a 40/60 PA66/sPS blend.

overlap of the diffraction patterns. For this reason, the WAXS crystallinity was determined only for compression-molded neat polymers: 30% for PA66 and 29% for sPS (WAXS provides distinctly lower values of crystallinity because DSC also records the enthalpy associated with imperfect, less ordered structures). A comparison of the diffraction patterns of the blends with those calculated under the assumption of additivity showed that the crystallinities of PA66 and sPS in the blends were not perceptibly affected by blending. On the other hand, the crystallite size (L_{110}) of sPS (evaluated at $2\theta = 6.7°$) increased with the sPS fraction in the blends as a result of the diminishing ratio of the compatibilizer to sPS (Table II). In contrast, no changes in $L_{010,110}$ of the PA66 crystallites (evaluated at $2\theta = 23.7°$) were observed.

DMTA

The dynamic mechanical patterns (Fig. 5) of the PA66/sPS blends showed three E'' peaks at about −70, 30, and 100°C. The latter two peaks corresponded to the glass (α) transitions of PA66 and sPS, respectively (Table II). The −70°C peak of the polyamides was induced by low-molar-mass diluents, that is, mainly by nonreacted monomer and absorbed water.[51,52] The high intensity of this secondary relaxation showed the presence of such diluents (to several percent[51]) in the PA66 component in the blends that were in equilibrium with the relative humidity (ca. 50%) at room temperature. These diluents also accounted for a relatively low glass-transition loss peak of PA66 detected by DMTA ($T_{\alpha 1}$) of 30°C in the blends. As the glass-transition temperature of PA66 (T_{g1}) of 63°C, recorded (Table I) in the second heating scan (of the specimens dried during the first heating scan), approached a real value,[53] we can presume that the depression of T_{g1} by about 20°C was mainly caused by absorbed water (no analysis of the low-molar-mass substances present in the PA66 component in the blends was carried out). The α loss peak of sPS was located at the relatively low glass-transition loss peak of sPS detected by DMTA ($T_{\alpha 2}$) of 98°C (Table II), which was in good agreement with DSC measurements indicating 94°C (Table I).

The two glass transitions of the studied blends were a result of their heterogeneity. The α loss peaks showed minor changes in their location on the temperature scale with the blend composition [Table II and Fig. 5(a)]: $T_{\alpha 2}$ somewhat rose with a decreasing sPS fraction in the blends, whereas $T_{\alpha 1}$ slightly decreased with a decreasing PA66 fraction. If the starting polymers were partially miscible, the PA66 peak would have shifted toward higher temperatures and the sPS peak would have shifted toward lower temperatures, but this was not the case. We suppose that the small rise in $T_{\alpha 2}$ (the 70/30 blend had a $T_{\alpha 2}$ value 7–9°C higher than that of sPS; Tables I and II) could be attributed to two effects. First, T_g of the homogeneous sPS/PPO blends was observed[48] to rise linearly with the PPO fraction (T_g of PPO ≈ 210°C); as our compatibilizer contained PPO and the compatibilizer/sPS ratio in the blends was rising with decreasing w_2 in the range $1 \leq w_2 \leq 0.3$, $T_{\alpha 2}$ slightly increased because of the mixing of PPO with sPS. Second, although the sPS

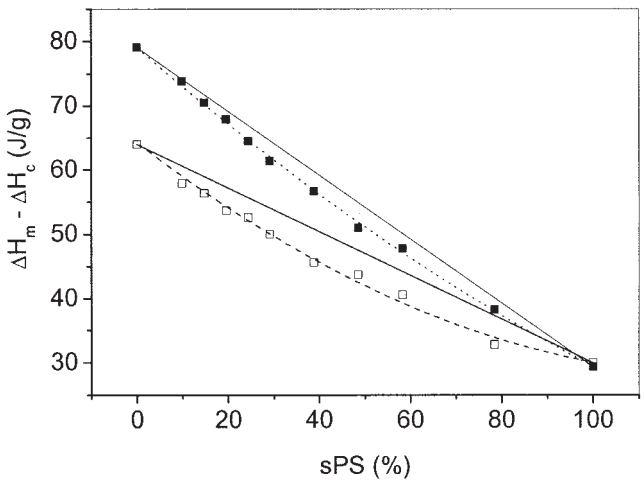

Figure 4 Difference between ΔH_m and ΔH_c, according to DSC measurements, for PA66/sPS blends. The parameters of eq. (1) were as follows: for the first heating scan, represented by a dashed line, P_1 was 0.17, P_2 was 0.33, C_1 was 0.34, and C_2 was 0.56; for the second heating scan, represented by a dotted line, P_1 was 0.10, P_2 was 0.18, C_1 was 0.42, and C_2 was 0.55. The full lines represent the additivity.

TABLE II
DMTA and WAXS Data of the PA66/sPS Blends as a Function of the Composition

PA66/sPS/C[a]	C/sPS (w/w)	$T_{\alpha 1}$ (°C)	E'' ($T_{\alpha 1}$; MPa)[b]	$T_{\alpha 2}$ (°C)	E'' ($T_{\alpha 2}$; MPa)[c]	WAXS crystal size (nm)[g]	
						PA66	sPS
100/0/0	—	30	152	—	—	6.3	—
90/10/1	0.100	29	147	107	39	6.8	—
85/15/1.5	0.100	29	148	107	48	7.1	18.6
80/20/2	0.100	28	138	107	55	7.0	16.4
75/25/2.5	0.100	24	135	107	57	7.1	16.0
70/30/3	0.100	24	141	107	71	6.8	21.9
60/40/3	0.077	23	126	104	105	7.2	25.6
50/50/3	0.059	23	114	104	134	6.9	29.6
40/60/3	0.050	23	101	104	179	7.1	31.3
20/80/2	0.025	24	64	101	239	6.1	30.9
0/100/0	0.000	—	—	98	332	—	30.0

[a] Blend composition (wt %); C = compatibilizer.
[b] Height of the glass-transition loss peak of PA66.
[c] Height of the glass-transition loss peak of sPS.
[d] Compare with Experimental section.

crystallite size remained approximately constant in the range of 100–50% sPS, it markedly decreased with a further decrease in the sPS fraction in the blends (Table II). In the latter interval, the relative sPS fraction contained in the interphase necessarily increased. As the interphase was a part of the noncrystalline regions, we could presume that the observed small increase in $T_{\alpha 2}$ with a decreasing sPS fraction also reflected an increasingly hindered mobility of tightened sPS chains in the interphase and its proximity.[54]

The decrease in $T_{\alpha 1}$ with a decreasing fraction of PA66 in the blends (Table II) could hardly be attributed to a rising concentration of water in the PA66 component because PA66 particles embedded in the sPS matrix were less accessible to air humidity. In our previous articles, we observed an analogous decrease in the glass-transition loss peak (T_α) of dispersed ethylene–propylene rubber with its diminishing fraction in binary blends with PP[55] or in ternary blends with PP and poly(styrene-*co*-acrylonitrile) (SAN).[30] The $T_{\alpha 1}$ depression could be explained as a result of the negative compression (acting on dispersed particles) that developed over the course of the cooling of the blend melt; the continuous matrix had a much higher $T_{\alpha 2}$ value than the dispersed component. Thus, in the $T_{\alpha 2} - T_{\alpha 1}$ interval, dispersed particles of PA66 shrank more, still being in the rubberlike state, than the glassy matrix. An increasing fraction of sPS in the blends enhanced the average negative pressure acting on PA66 particles. However, as the observed effect was very small and irrelevant for other mechanical properties, it was not analyzed in greater detail.

The corresponding temperature dependence of E' [Fig. 5(b)] indicated that the values of E' at $T_{\alpha 1}$ or $T_{\alpha 2}$ were almost independent of the blend composition. To better visualize the effect of the blend composition on E' at various temperatures, we plotted the data extracted from Figure 5(b) in Figure 6. The latter graph is essential from the viewpoint of conceivable applications of PA66/sPS blends: although E'(25°C) was virtually independent of the blend composition, E'(75°C) markedly rose with the sPS fraction (which held for the modulus in the central interval of 25–100°C). However, E'(125°C) was low and noticeably decreased with the percentage of sPS in the blends; this showed, contrary to expected results, that sPS did not impart a better dimensional stability to the blends with PA66 at elevated temperatures.

Tensile creep

The dependence of the tensile compliance [$D(t)$] encompassing the time interval from 10^{-1} to 10^4 min is given for selected blends in Figure 7. By chance, $T_{\alpha 1}$ was close to the temperature of the creep measurements, and so the observed differences in the compliance of the blends were relatively small [Fig. 5(b)]. For this reason, initial values of $D(t = 6\ \text{s})$ were located in a narrow interval, which broadened with the elapsed time of creep. The log $D(t)$–log t plots of the experimental data were approximated by straight lines,[56–58] the slope of which was proportional to the creep rate. Generally, the compliance and creep rate of the blends decreased with the sPS fraction. Although the compliance of PA66 increased by an order of magnitude over the measured time interval, the compliance of sPS was virtually time-independent. However, because of the inherent brittleness and low tensile strength of sPS and the blends with a high percentage of sPS, creep measurements could be implemented only with low values of stress. The 60/40 and 50/50 PA66/sPS blends, that is, materials with cocontinuous compo-

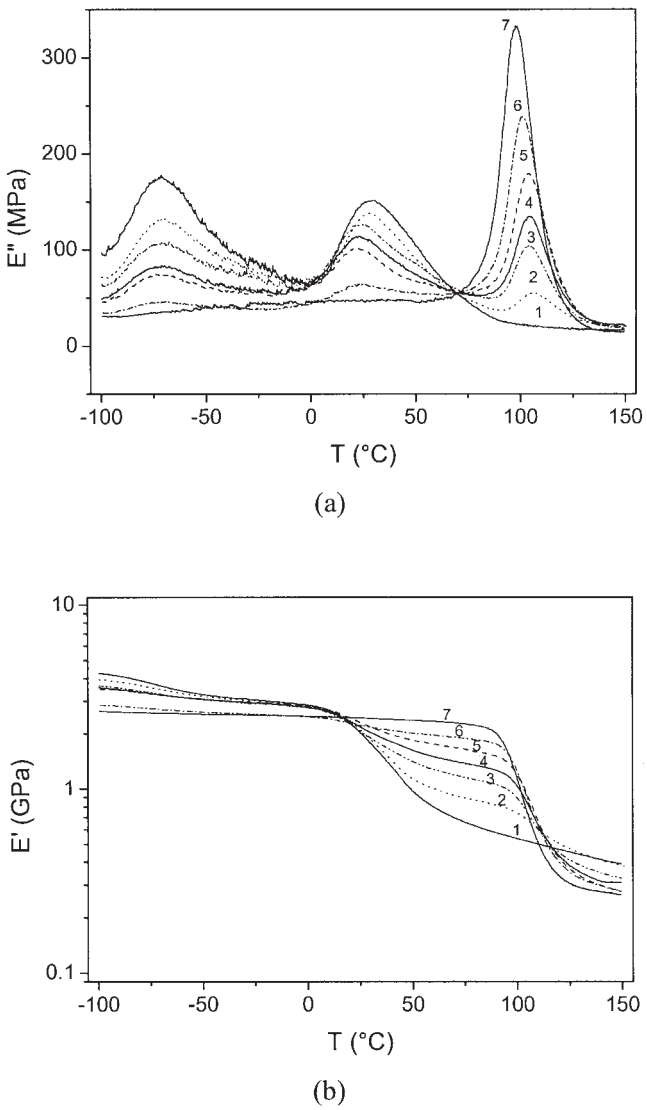

Figure 5 Effect of the composition (wt %) of PA66/sPS blends on the temperature dependence of (a) E'' and (b) E': (1) 100/0, (2) 80/20, (3) 60/40, (4) 50/50, (5) 40/60, (6) 20/80, and (7) 0/100 PA66/sPS.

nents, showed a conspicuous rise in their creep rate for the periods exceeding 1000 min. We observed an analogous effect for the PP/SAN blends[57] that we explained by a time-dependent redistribution of the stresses acting on the cocontinuous fractions of the constituents during the course of the creep of the blends. The blends containing 60 or 80% sPS displayed a reduced creep rate but also a low tensile strength (Table III), which most likely preclude their applications.

Stress–strain and impact measurements

The obtained results, summarized in Table III, show that the tensile modulus (E) and S_y consistently grew with the concentration of sPS in the blends. In parallel, the yield strain (e_y) steeply decreased, and so no yielding was observed for sPS and the 20/80 PA66/sPS blend. The stress at break (S_u) displayed a small local maximum at 25–30% sPS; as the strain at break (e_u) simultaneously passed through a prominent maximum, the tensile energy to break (TEB) was characterized by a maximum in this range. However, a further increase in the sPS fraction in the blends accounted for a profound drop in e_u and TEB. TIS decreased monotonically, but steeply, with the fraction of sPS in the blends.

CONCLUSIONS

The integral crystallinity of the PA66 and sPS components in their blends was virtually unaffected by the blend composition. However, DSC measurements revealed that the crystallinity strongly depended on the cooling rate. Two melting peaks indicating the polymorphism of sPS were observed for blends containing more than $w_2 = 0.50$. In the composition interval $0 < w_2 \leq 0.30$, sPS was dispersed in the PA66 matrix, whereas the blends with $0.40 \leq w_2 \leq 0.60$ showed partially cocontinuous components, and PA66 contained small particles of sPS and vice versa. For $w_2 > 0.60$, PA66 was dispersed in a continuous sPS matrix. Fracture surfaces in compatibilized blends advanced not along the interface but through both components, and this suggested that the interfacial adhesion was high enough to prevent debonding of the blend constituents.

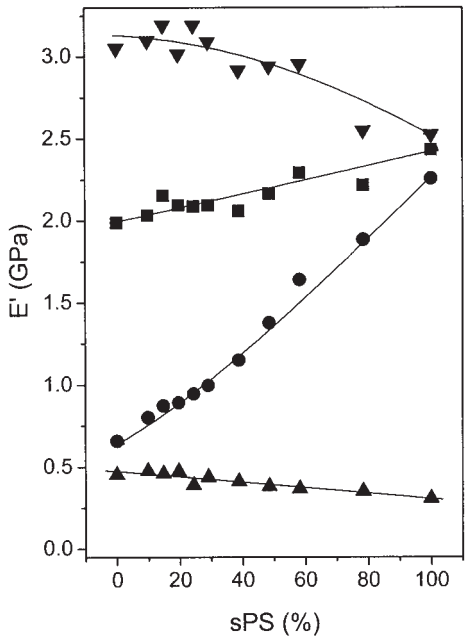

Figure 6 E' of PA66/sPS blends as a function of the composition at selected temperatures: (▼) −75, (■) 25, (●) 75, and (▲) 125°C.

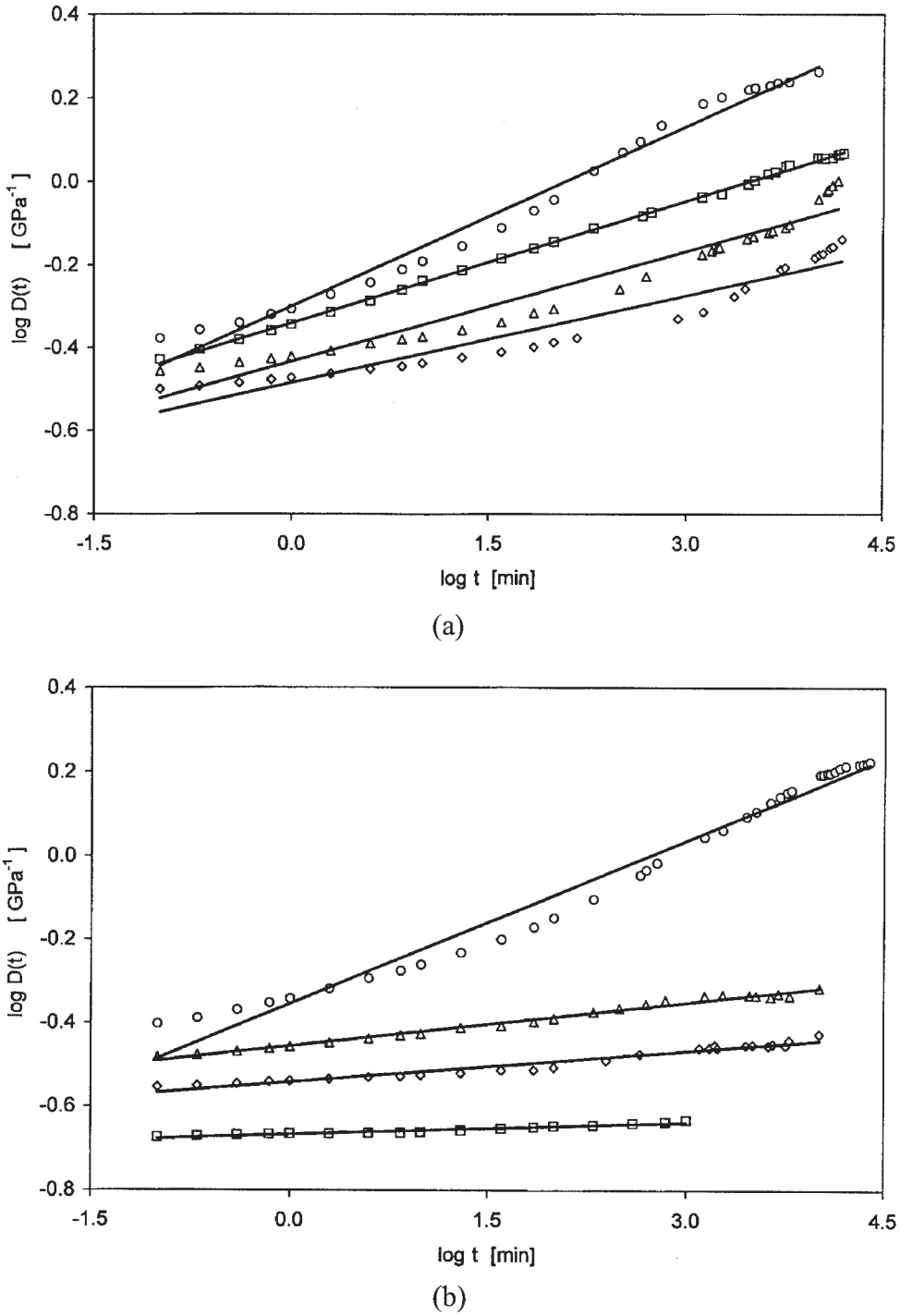

Figure 7 Effect of the composition (wt %) of PA66/sPS blends on the time dependence of $D(t)$: (a) (○) 100/0, (□) 70/30, (△) 60/40, and (◇) 50/50 PA66/sPS and (b) (○) 80/20, (□) 40/60, (△) 20/80, and (◇) 0/100 PA66/sPS.

All the mechanical properties of the PA66/sPS blends were profoundly affected by the blend composition. Dynamic mechanical measurements showed that E' (25°C) was virtually independent of the blend composition, whereas E'(75°C) rose with the sPS fraction (which applied to the modulus in the whole interval of 25–100°C). However, E' (125°C) noticeably declined with the percentage of sPS in the blends, and this meant that sPS did not impart better dimensional stability to the blends at elevated temperatures. The compliance of PA66 rose by an order of magnitude over the measured time interval of 0.1–10 000 min, whereas the compliance of sPS was virtually time-independent; consequently, the compliance and creep

TABLE III
Mechanical Properties of the PA66/sPS Blends

PA66/sPS/C[a]	E (GPa)	S_y (MPa)	e_y (%)	S_u (MPa)	e_u (%)	TEB (MPa)	TIS (kJ/m^2)
100/0/0	1.27	42.8	32.5	69.5	233	47.7	213.2
90/10/1	1.35	48.7	18.2	31.6	38.9	9.12	128.1
85/15/1.5	1.70	50.1	17.9	35.3	65.2	11.5	135.0
80/20/2	1.59	51.0	16.5	45.8	80.8	17.5	121.1
75/25/2.5	1.68	50.8	13.4	59.4	152.8	31.7	108.3
70/30/3	1.92	52.7	9.2	57.8	136.8	28.2	88.0
60/40/3	2.04	56.7	4.6	52.0	67.0	12.6	72.6
50/50/3	2.02	56.5	4.1	46.5	46.2	8.00	30.1
40/60/3	2.24	61.5	3.9	54.5	5.8	0.77	27.5
20/80/2	2.49	—	—	52.8	2.1	0.22	26.9
0/100/0	3.03	—	—	48.8	1.7	0.17	9.5

[a] Blend composition (wt %); C = compatibilizer.

rate of the blends decreased proportionally to the sPS fraction. Also, E and S_y consistently grew with the sPS content in the blends; in parallel, e_y steeply decreased, and so no yielding was observed for blends containing more than 60% sPS. S_u, e_u, and TEB displayed local maxima at 25–30% sPS; blends with more than 60% sPS were brittle, showing very low values of the ultimate properties. TIS decreased steeply, but monotonically, with the fraction of sPS in the blends.

The authors very much appreciate the assistance of Josef Baldrian (for the wide-angle X-ray scattering measurements), V. Hašová (for the preparation of the blends and the measurement of the tensile impact strength), and L. Kaprálková (for the Instron measurements).

References

1. Wesson, R. D. Polym Eng Sci 1994, 34, 1157.
2. Woo, E. M.; Wu, F. S. Macromol Chem Phys 1998, 199, 2041.
3. Malanga, M. Adv Mater 2000, 12, 1869.
4. Chiu, F. C.; Peng, C. G.; Fu, Q. Polym Eng Sci 2000, 40, 2397.
5. Yuan, Z.; Song R.; Shen, D. Polym Int 2000, 49, 1377.
6. Sun, Y. S.; Woo, E. M. Polymer 2001, 42, 2241.
7. Li, Y.; He, J.; Qiang, W.; Hu, X. Polymer 2002, 43, 2489.
8. Sudduth, R. D.; Kyarala, P.; Sheng, Q. Polym Eng Sci 2002, 42, 694.
9. Cimmino, S.; DiPace, E.; Martuscelli, E.; Silvestre, C. Polymer 1993, 34, 2799.
10. Hwang, S. H.; Kim, Y. S.; Cha, H. C.; Jung, J. C. Polymer 1999, 40, 5957.
11. Duff, S.; Tsuyama, S.; Iwamoto, T.; Fujibayashi, F.; Birkinshaw, C. Polymer 2001, 42, 991.
12. Koh, K. A.; Kim, J. H.; Lee, D. H.; Lee, M.; Jeong, H. M. Eur Polym J 1998, 34, 1229.
13. Hong, B. K.; Jo, W. H. Polymer 2000, 41, 2069.
14. Xu, S.; Chen, B.; Tang, T.; Huang, B. Polymer 1999, 40, 3399.
15. Ramsteiner, F.; McKee, G. E.; Heckmann, W.; Oepen, S.; Geprags, M. Polymer 2000, 41, 6635
16. Choi, S. H.; Cho, I.; Kim, K. U. Polym J 1999, 31, 828.
17. Abis, L.; Abbondanza, L.; Braglia, R.; Castellani, L.; Giannotta, G.; Po, R. Macromol Chem Phys 2000, 201, 1732.
18. Chen, B.; Li, X.; Xu, S.; Tang, T.; Zhou, B.; Huang, B. Polymer 2002, 43, 953.
19. Li, H. M.; Shen, Z. G.; Zhu, F. M.; Lin, S. A. Eur Polym J 2002, 38, 1255.
20. Chen, B.; Tang, T.; Su, S. Q.; Zhang, X. Q.; Huang, B. T. Polym J 2003, 35, 141.
21. Xu, D.; Wang, J.; Liu, Z.; Ke, Y.; Hu, Y. Macromol Chem Phys 2001, 202, 1817.
22. Park, C. I.; Park, O. O.; Lim, J. G.; Kim, H. J. Polymer 2001, 42, 7465.
23. Tseng, C. R.; Wu, J. Y.; Lee, H. Y.; Chang, F. C. Polymer 2001, 42, 10063.
24. Kolařík, J. Polym Eng Sci 1996, 36, 2518.
25. Kolařík, J. Eur Polym J 1998, 34, 585.
26. Matsuoka T.; Yamamoto, S. J Appl Polym Sci 1998, 68, 807.
27. Willemse, R. C.; de Boer, A. P.; van Dam, J.; Gotsis, A. D. Polymer 1998, 39, 5879.
28. Willemse, R. C. Polymer 1999, 40, 2175.
29. Veenstra, H.; van Dam, J.; de Boer, A. P. Polymer 1999, 40, 1119.
30. Kolařík, J.; Pegoretti, A.; Fambri, L.; Penati, A. J Polym Res 2000, 7, 7.
31. Kolařík, J.; Fambri, L.; Pegoretti, A.; Penati, A. Polym Eng Sci 2000, 40, 127.
32. Xu, B.; Simonsen, J.; Rochefort, W. E. J Appl Polym Sci 2000, 76, 1100.
33. Steinmann, S.; Gronski, W.; Friedrich, C. Polymer 2001, 42, 6619.
34. Lyngaae-Jorgensen, J.; Utracki, L. A. Polymer 2003, 44, 1661.
35. Horský, J.; Kolařík, J.; Fambri, L. Macromol Mater Eng 2001, 286, 216.
36. Okada A.; Masuyama, A. U.S. Pat. 5,326,813 (1994).
37. Wünsch, J.; Gottschalk, A.; Weber, M.; Altstädt, M.; Kressler, J.; Thomann, R. Int. Pat. WO 97/11123 (1997).
38. Jo, W. H.; Park, C. D.; Lee, M. S. Polymer 1996, 37, 1709.
39. Ide, F.; Hasagawa, A. J Appl Polym Sci 1974, 18, 963.
40. Chang, F. G.; Hwu, Y. C. Polym Eng Sci 1991, 31, 1509.
41. Montezinos, D.; Wells, B. G.; Burns, J. L. J Polym Sci Polym Lett Ed 1985, 23, 421.
42. Brown, G. M.; Buttler, J. H. Polymer 1997, 38, 3937.
43. Alexander, L. E. X-Ray Diffraction Methods in Polymer Science; Wiley-Interscience: New York, 1969.
44. Van Krevelen, D. W. Properties of Polymers; Elsevier: Amsterdam, 1990.
45. Pastor, J. R.; Landes, B. G.; Karjala, P. J. Thermochim Acta 1991, 187, 195.
46. Shibata, M.; Yosomiya, R.; Jiang, Z.; Yang, Z.; Wang, G.; Ma, R.; Wu, Z. J Appl Polym Sci 1999, 74, 1686.
47. Minkova, L.; Yordanov, H.; Filippi, S. Polymer 2002, 43, 6195.

48. Guerra, G.; De Rosa, C.; Vitagliano, V. M.; Petraccone, V.; Corradini, P. J Polym Sci Part B: Polym Phys 1991, 29, 265.
49. Hong, B. K.; Jo, W. H.; Lee, S. C.; Kim, J. Polymer 1998, 39, 1793.
50. Woo, E. M.; Sun, Y. S.; Lee, M. L. Polymer 1999, 40, 4425.
51. Kolařík, J.; Janáček, J. J Polym Sci Part C: Polym Symp 1967, 16, 441
52. McCrum, N. G.; Read B. E.; Williams, G. Anelastic and Dielectric Effects in Polymeric Solids; Wiley: New York, 1967.
53. Kohan, M. I. Nylon Plastics; Wiley: New York, 1973.
54. Struik, L. C. E. Physical Aging of Amorphous Polymers and Other Materials; Elsevier: Amsterdam, 1978.
55. Kolařík, J.; Agrawal, G. L.; Kruliš, Z.; Kovář, J. Polym Compos 1986, 7, 463.
56. Kolařík, J. J Polym Sci Part B: Polym Phys 2003, 41, 736.
57. Kolařík, J.; Pegoretti, A.; Fambri, L.; Penati, A. J Appl Polym Sci 2003, 88, 641.
58. Kolařík, J.; Pegoretti, A.; Fambri, L.; Penati, A. Macromol Mater Eng 2003, 288, 629.